

1
2
3
4
5
6
7
8
9
10
11
12
13
14
15
16
17
18
19
20
21

Geophysical Research Letters

Supporting Information for

Major modes of climate variability dominate nonlinear Antarctic ice-sheet elevation changes 2002-2020

Matt A. King^{1,2}, Poul Christoffersen^{2,3}

¹School of Geography, Planning, and Spatial Sciences, University of Tasmania, Hobart, Tasmania 7001, Australia

²The Australian Centre for Excellence in Antarctic Science, University of Tasmania, Hobart, Tasmania 7001, Australia

³Institute for Marine and Antarctic Studies, University of Tasmania, Hobart, Tasmania 7001, Australia

Contents of this file

- Text S1
- Figures S1 to S9
- Table S1

22 **Text S1**

23

24 To make a first-order estimate of plausible velocity-driven changes on surface elevation on Pine
 25 Island and Thwaites Glacier, we used annual Measures v2 ice velocities (Rignot et al., 2017) to
 26 derive year-on-year velocity changes at the glacier point positions where we extracted time series
 27 of surface elevation changes (shown in Fig. 3). The annual velocity changes were extracted in
 28 polar stereographic coordinates (x, y) and averaged over a 25 × 25 km box centred around each
 29 of the two geographical locations. The corresponding changes in surface height were estimated
 30 from the conservation of mass:

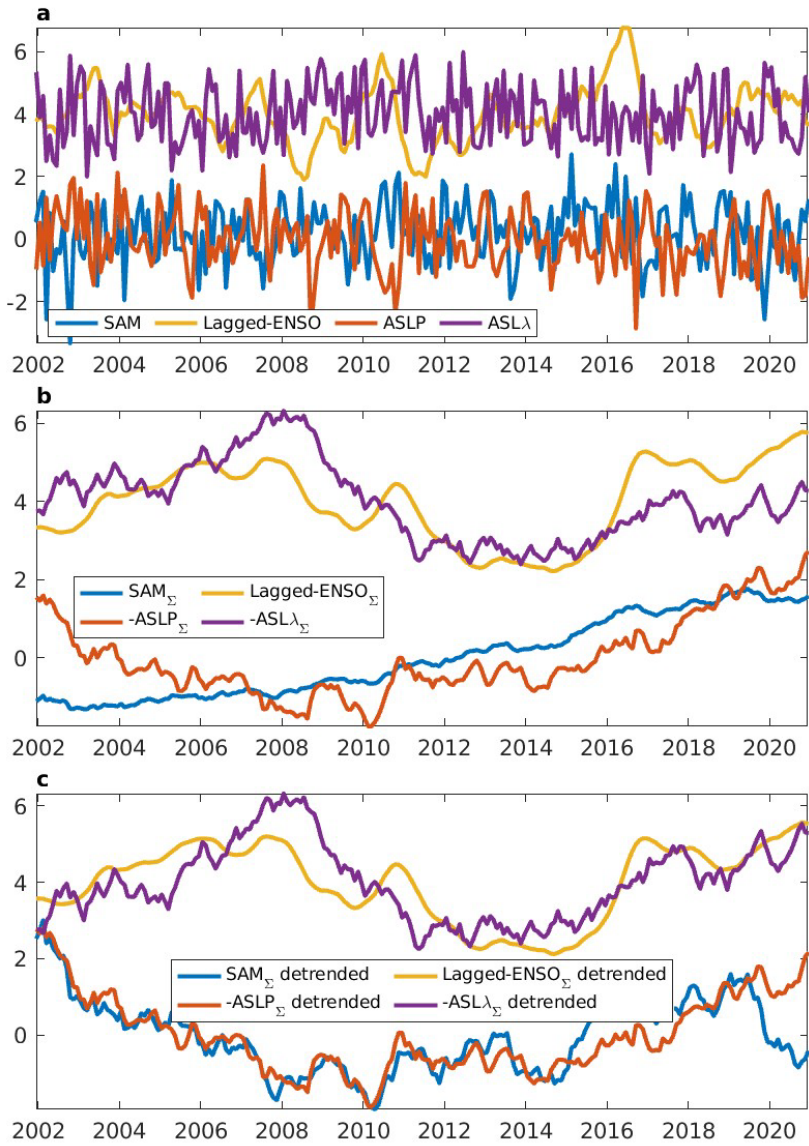
31
$$\frac{\partial h}{\partial t} = \dot{a} + \dot{b} + \bar{v} \cdot \nabla H + H \cdot \dot{\epsilon}_z$$

32 where \dot{a} is the surface accumulation from snowfall, \dot{b} is the basal accumulation when water at
 33 the bed freezes on (negative for melting), \bar{v} is the velocity vector, ∇ is the gradient operator, H is
 34 ice thickness and $\dot{\epsilon}_z$ is the vertical strain rate averaged for the ice column. We used the third and
 35 fourth term on the RHS to derive estimates of the elevation change stemming specifically from
 36 the change in velocity, ignoring the accumulation terms \dot{a} and \dot{b} . If the velocity change is $\delta\bar{v}$, the
 37 change in height is $-\delta\bar{v} \cdot \nabla H + H \cdot \delta\dot{\epsilon}_z$, where the first term denotes elevation gain from
 38 advection of thicker ice (or the opposite) and the second term is elevation loss due to dynamic
 39 thinning when the ice velocity increases (or the opposite). The change in velocity, $\delta\bar{v} =$
 40 $(\Delta v_x, \Delta v_y)$ was the annual difference from one year to the next. The advection term was
 41 calculated as $\Delta v_x dh/dx + \Delta v_y dh/dy$, while strain thinning was calculated as
 42 $H(-\Delta(dv_x/dx) - \Delta(dv_y/dy))$ with the assumption that ice is incompressible ($\delta\dot{\epsilon}_z = -\delta\dot{\epsilon}_x -$
 43 $\delta\dot{\epsilon}_y$) and vertical strain in the ice column is uniform. Fig. S9 shows the estimated elevation
 44 change in terms of advection and strain and their total with a Gaussian filter applied to the
 45 velocity vector \bar{v} .

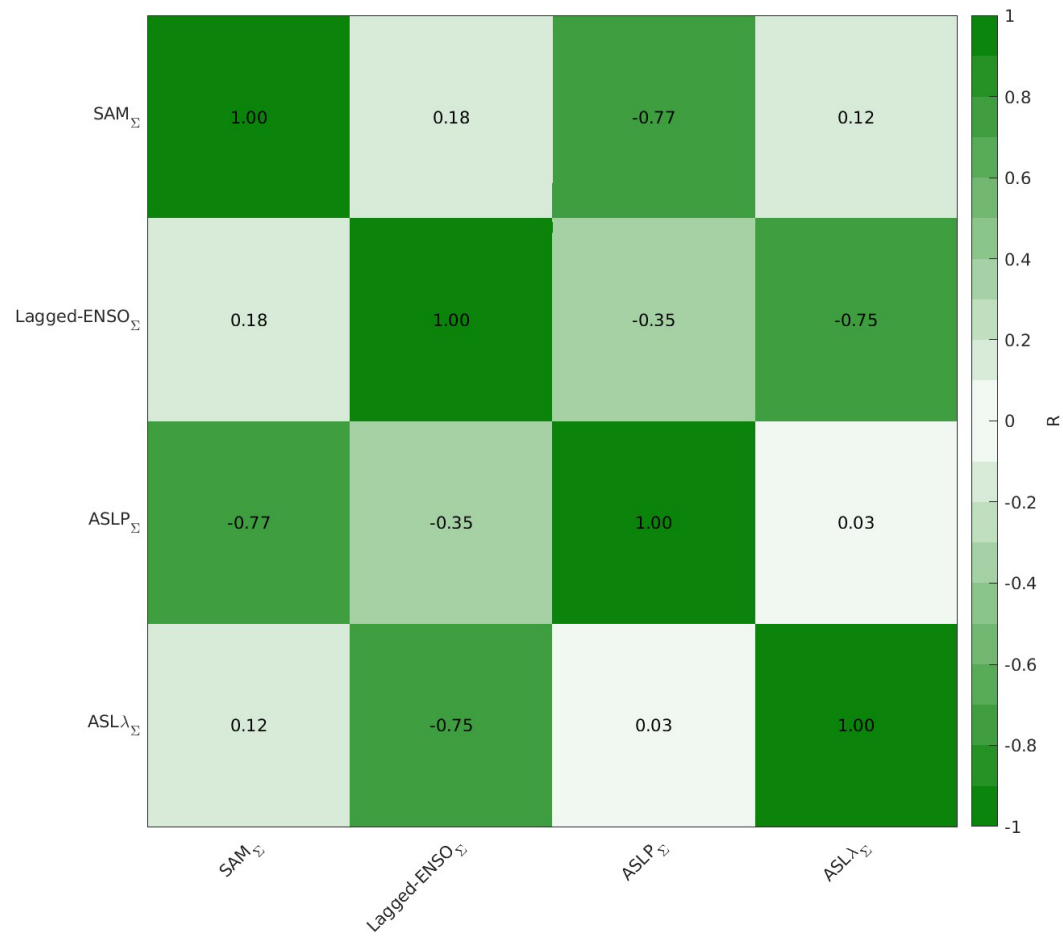
46

47

48
49 Supplementary Figures
50
51



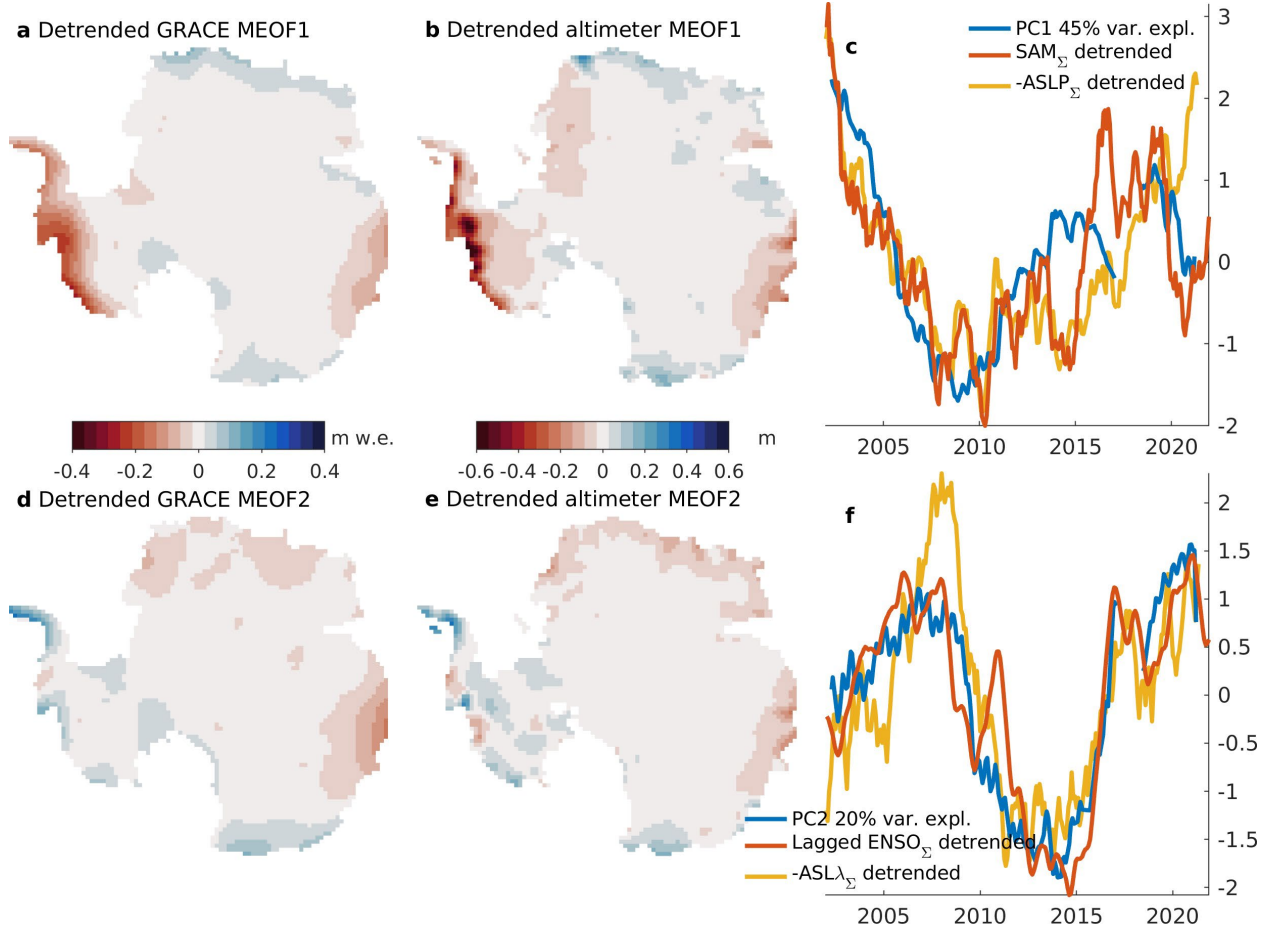
52
53 **Fig S1.** Cumulatively summed and detrended climate indices. The panels show the normalized
54 climate indices (a), their cumulative sum renormalized (b), after further detrending and
55 renormalization (c). ENSO and ASL λ terms are shown offset by 4 units for clarity.
56
57



59
60
61
62

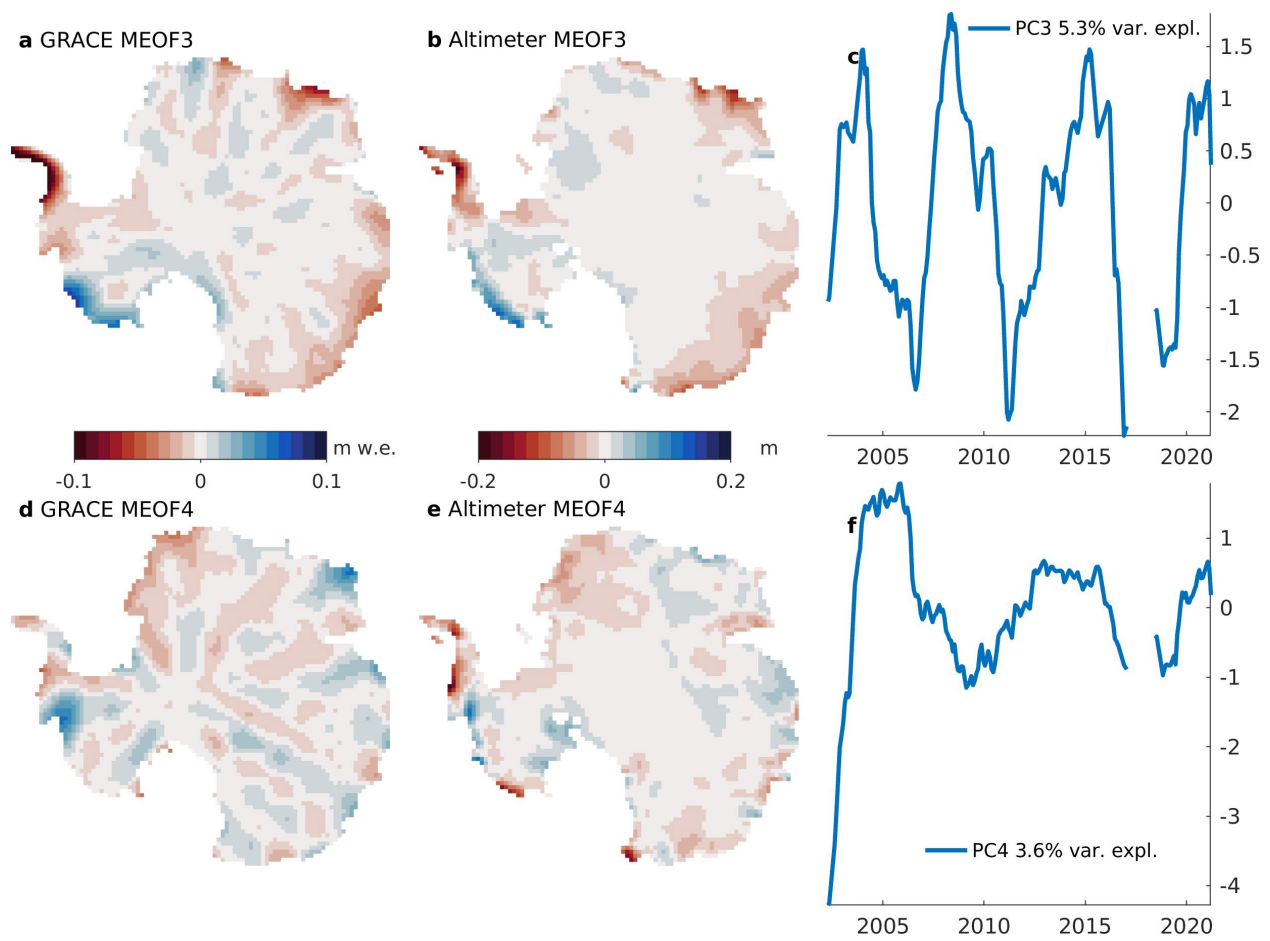
Fig S2. Correlation coefficients of summed and detrended climate indices.

63
64



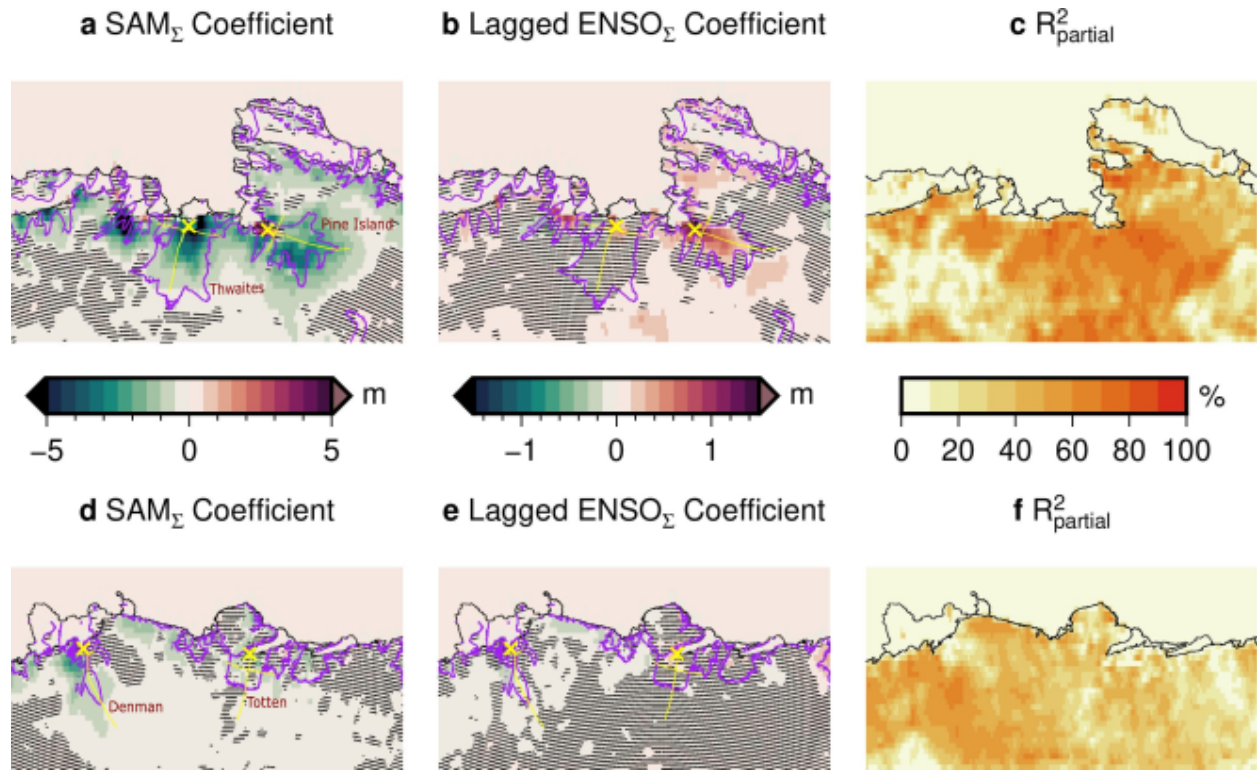
65
66
67
68
69
70
71

Fig S3. The leading two modes of the detrended altimeter and GRACE data based on MVEOF. The EOFs are shown after scaling to reverse the effects of normalization. GRACE modes (a, d) are shown in units of meters of water equivalent (w.e.), and altimeter modes (b, e) shown in units of meters of ice elevation. Overlain on PC1 is the detrended SAM_{Σ} and $-ASLP_{\Sigma}$ indices and overlay on PC2 is the lagged $ENSO_{\Sigma}$ and $-ASL_{\Sigma}$. The variances explained by each mode are indicated in the legends of panels c and f.



72
73
74
75
76
77
78

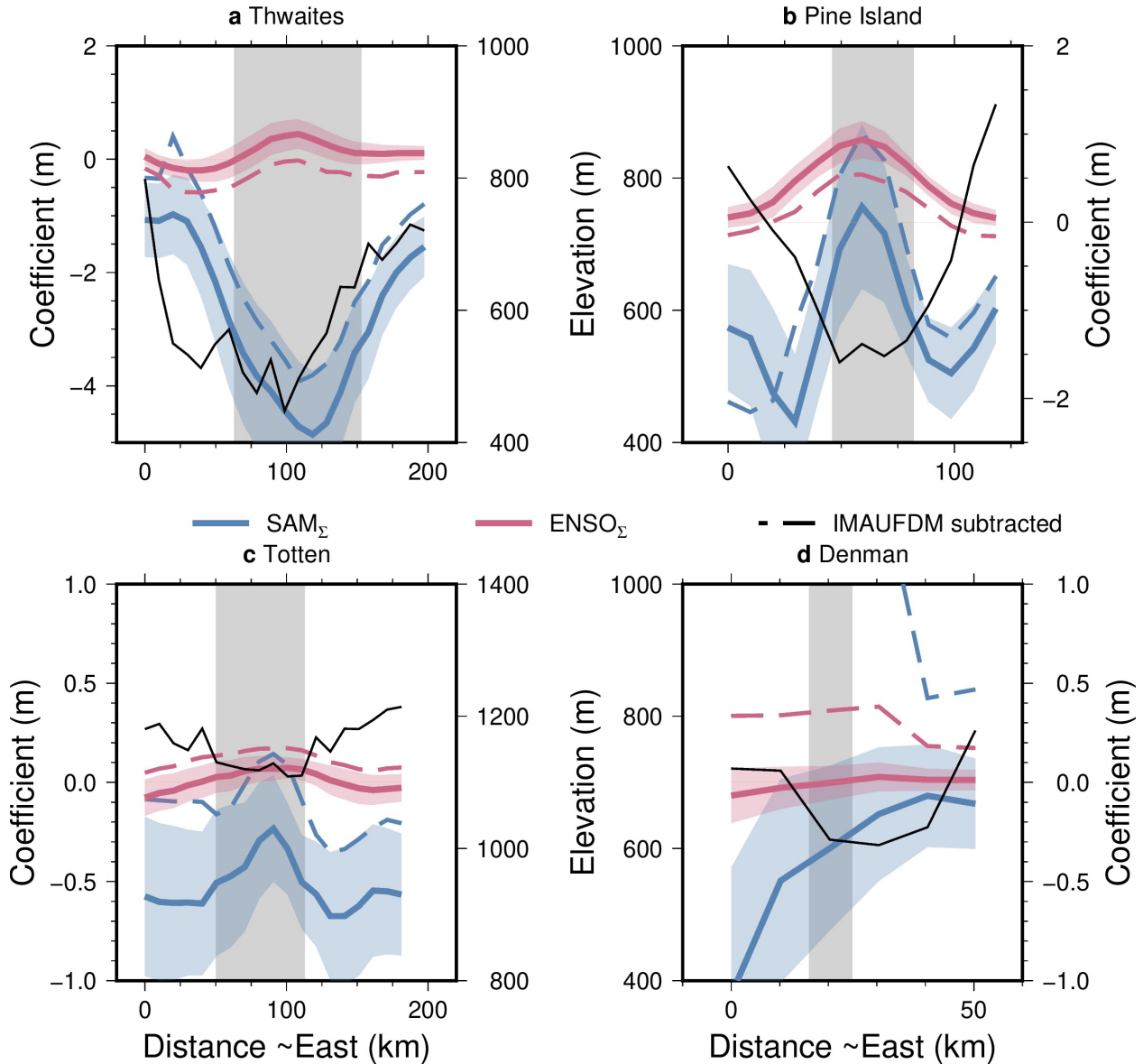
Fig S4. Modes 3 and 4 of the MVEOF. Note the changes in color scale from Fig S3.



79
80
81
82
83
84
85
86
87

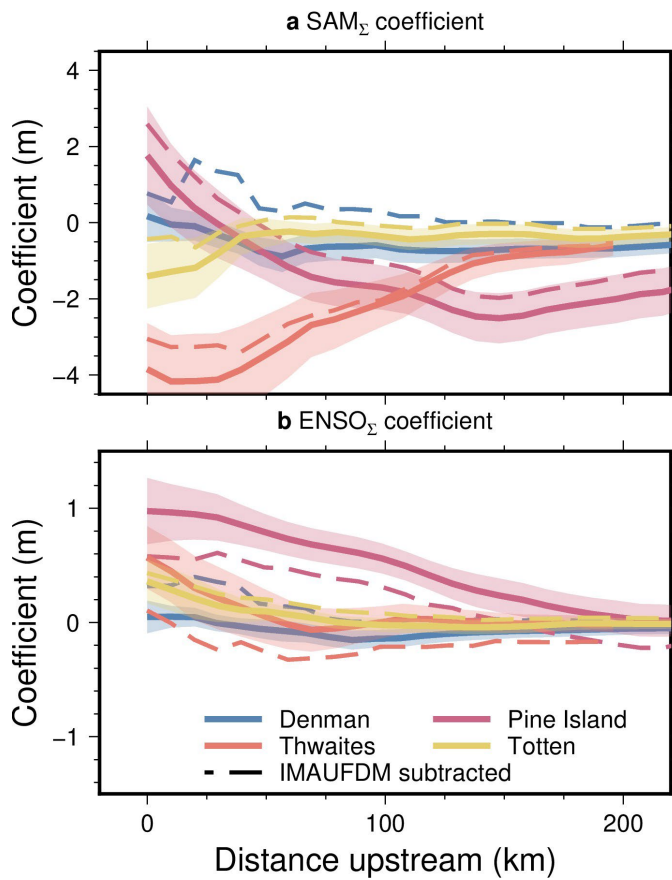
Fig S5. Detail of Figure 1 in the Amundsen Sea Embayment (top) and Denman-Totten glacier (bottom) regions. Thick black lines show the grounding line and thin black lines the ice shelf limits (Haran et al., 2014, updated 2019). Pink lines define the 100 m/yr speed contour (Rignot et al., 2017). Yellow lines mark the locations of ice stream profiles and yellow cross marks the location of the ice stream time series.

88
89
90



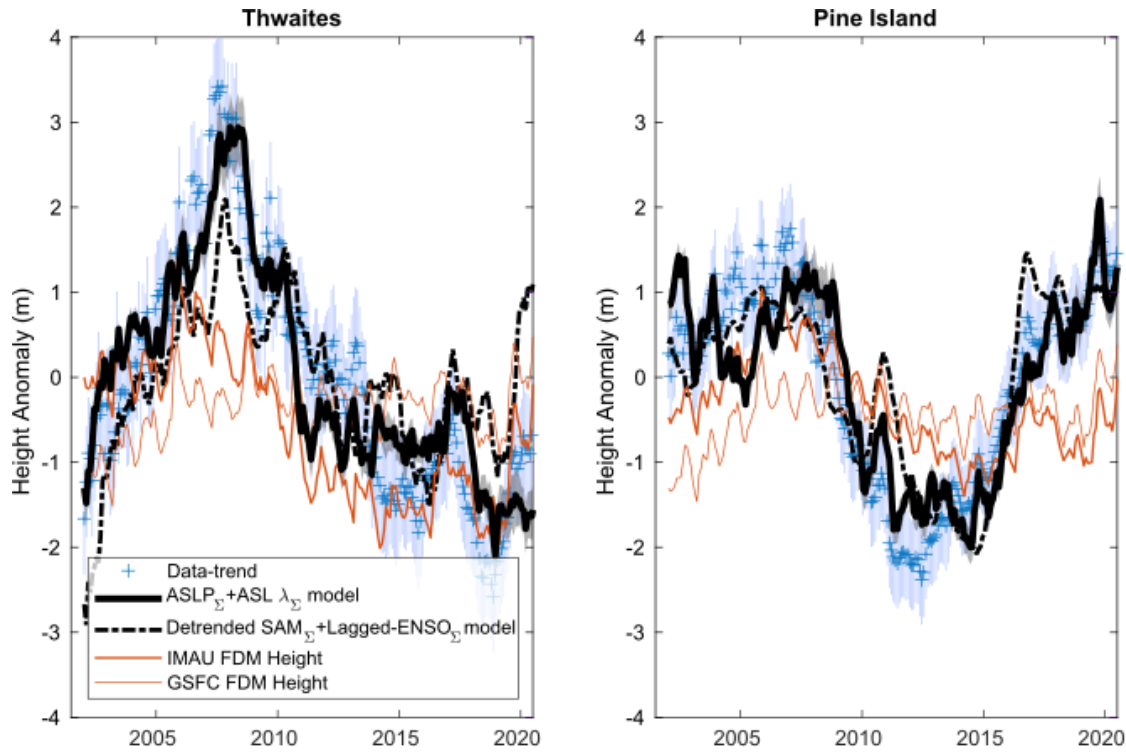
91
92
93
94
95
96
97
98
99
100
101
102

Fig S6. Cross-section profiles of SAM Σ (a) and ENSO Σ (b) coefficients as a function of distance across Thwaites (a), Pine Island (b), Totten (c) and Denman (d) glaciers. Coefficients are shown as estimated before (colored solid line) and after (colored dashed line) subtraction of the IMAU FDM. The ice elevation extracted from the REMA v2.0 1 km mosaic (Howat, 2022) is shown as a black line (central axes). Colored shading indicates the 1-sigma confidence limits. The vertical grey box indicates the 100 m/yr limits of ice flow based on Measures v2. The locations of the profiles are shown in Figure S5 as yellow lines.

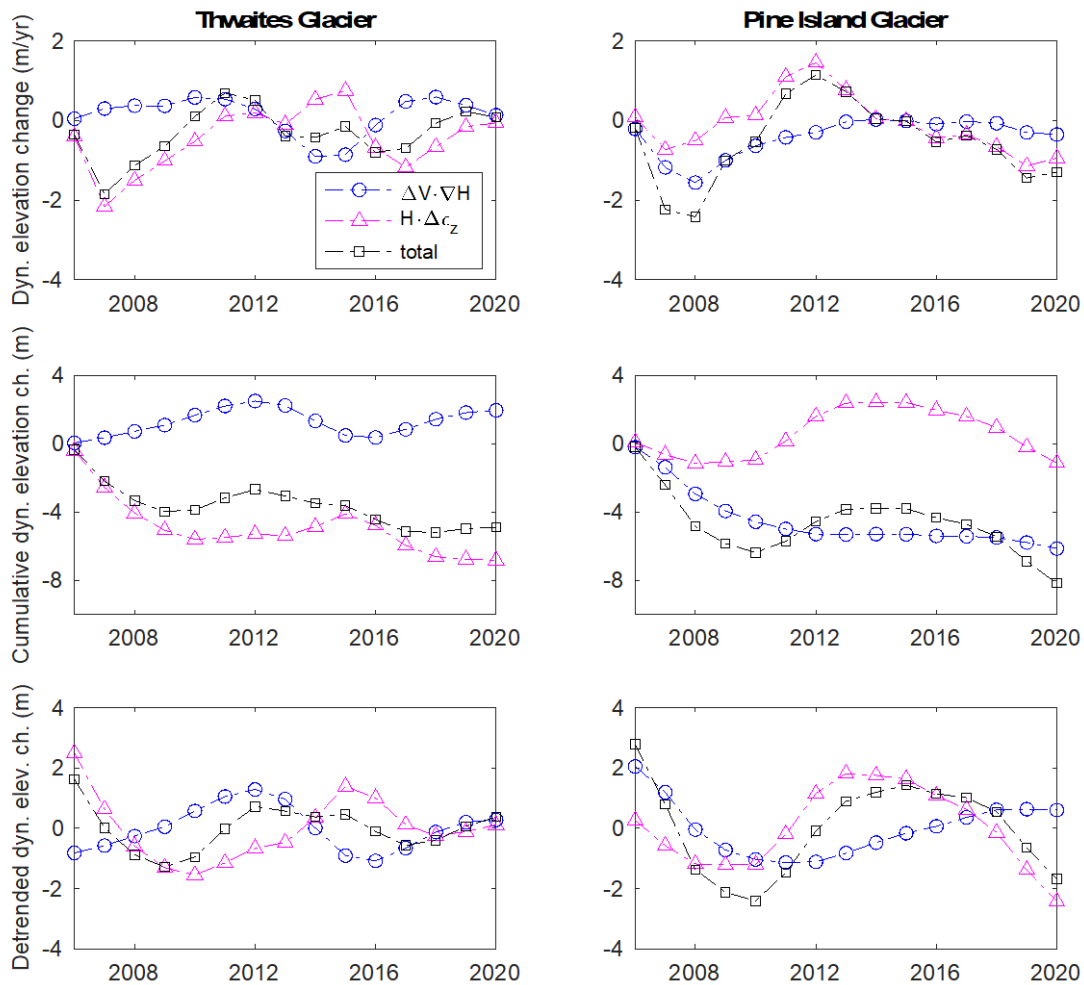


103
 104
 105
 106
 107
 108
 109
 110

Fig S7. Centre-line profiles of SAM_{Σ} (a) and $ENSO_{\Sigma}$ (b) coefficients as a function of distance upstream of the grounding line of major ice streams. Coefficients are shown before (solid line) and after (dashed line) subtraction of the IMAU FDM. Shading indicates the 1-sigma confidence limits. The locations of the profiles are shown in Figure S5 as yellow lines.



111
 112 **Figure S8.** As for Figure 3 but showing only the Thwaites and Pine Island time series. Panels
 113 show (left axes) the detrended data and their 2-sigma uncertainties (blue pluses and error bars),
 114 outputs of two models of firn densification (FDM; brown lines), the best fitting models based on
 115 ASL (black solid line with 2-sigma uncertainty in gray shading) and SAM+ENSO (black dashed
 116 lines) terms.
 117



118
 119 **Figure S9.** Dynamic elevation change derived from mass conservation and observed changes in
 120 the flow of Thwaites Glacier (left) and Pine Island Glacier (right) since 2006. The annual
 121 elevation change ($\delta h/\delta t$, top row) from flow of ice alone (black line) is the sum of advective
 122 thickness change (blue line) and strain (magenta line) tied to the change in velocity and vertical
 123 strain from one year to the next. Estimates are mean values for a 25 x 25 km box centered around
 124 each glacier point used in Figure 3 and given in Table S1. Also shown are δh (middle) and
 125 detrended δh (bottom). The input data are MEaSUREs surface velocities provided in polar
 126 stereographic coordinates and interpolated onto a 500 m grid and filtered. Ice thickness is
 127 ‘Bedmachine Antarctica’ version 3. Other sources of elevation change are ignored. See Text S1
 128 for method and details.

129

130 Table S1

131

132 **Table S1.** Location in Antarctic Polar Stereographic coordinates (EPSG:3031) of sites in Fig. 3
133 and Fig S8 and discussed in the main text.

Glacier	X(m)	Y(m)
Thwaites	-1511702	-463473
Pine Island	-1583860	-232513
Totten	2274795	-988293
Denman	2496950	-423352

134